JOURNAL OF AIRCRAFT
Vol. 46, No. 4, July–August 2009

Nonlinear Reduced-Order Analysis with Time-Varying Spatial Loading Distributions

Adam Przekop*
Analytical Services and Materials, Inc., Hampton, Virginia 23666
and
Stephen A. Rizzi†
NASA Langley Research Center, Hampton, Virginia 23681

DOI: 10.2514/1.39790

Oscillating shocks acting in combination with high-intensity acoustic loadings present a challenge to the design of resilient hypersonic-flight vehicle structures. This paper addresses some features of this loading condition and certain aspects of a nonlinear reduced-order analysis with emphasis on system identification, leading to the formation of a robust modal basis. The nonlinear dynamic response of a composite structure subject to the simultaneous action of locally strong oscillating pressure gradients and high-intensity acoustic loadings is considered. The reduced-order analysis used in this work has been previously demonstrated to be both computationally efficient and accurate for time-invariant spatial loading distributions, provided that an appropriate modal basis is used. The challenge of the present study is to identify a suitable basis for loadings with time-varying spatial distributions. Using a proper orthogonal decomposition and modal expansion, it is shown that such a basis can be developed. The basis is made more robust by incrementally expanding it to account for changes in the location, frequency, and span of the oscillating pressure gradient.

Nomenclature

a	=	quadratic modal stiffness coefficient
b	=	cubic modal stiffness coefficient
$[C]$, $[\tilde{C}]$	=	damping matrix in physical degrees of freedom and modal coordinates
d	=	linear modal stiffness coefficient
$\{f\}$, $\{\tilde{f}\}$	=	force vector in physical degrees of freedom and modal coordinates
$\{f_{NL}\}$, $\{\tilde{f}_{NL}\}$	=	restoring force vector in physical degrees of freedom and modal coordinates
$[I]$	=	identity matrix
L	=	number of modal basis functions
M	=	number of most contributing proper orthogonal modes
$[M]$, $[\tilde{M}]$	=	mass matrix in physical degrees of freedom and modal coordinates
m	=	number of nodes in finite element model
N	=	number of physical degrees of freedom
n	=	number of displacement fields used in snapshot matrix
$[P]$, $\{p\}$	=	matrix of proper orthogonal modes, proper orthogonal mode vector
q	=	modal (generalized) coordinate
$[R]$	=	correlation matrix
$[S]$, $\{s\}$	=	matrix of modal expansion coefficients, vector of modal expansion coefficients
t	=	time
u, v, w	=	displacement components in the x, y, and z directions
υ	=	cumulative proper orthogonal mode participation factor
$[X]$, $\{x\}$	=	displacement snapshot matrix, displacement time-history vector
ζ	=	viscous damping factor
$[\lambda]$	=	proper orthogonal value matrix
$[\Phi]$, $\{\phi\}$	=	matrix of normal modes, normal mode vector
χ_i	=	ith proper orthogonal mode participation factor
ω	=	undamped natural frequency

Presented as Paper 2323 at the 49th Structures, Structural Dynamics, and Materials Conference, Schaumburg, IL, 7–10 April 2008; received 3 October 2008; revision received 23 April 2009; accepted for publication 27 April 2009.

*Senior Structural Engineer, 107 Research Drive. Senior Member AIAA.
†Aerospace Engineer, Structural Acoustics Branch, Mail Stop 463. Associate Fellow AIAA.

I. Introduction

DESPITE the fact that commercial off-the-shelf finite element (FE) tools exist for time-domain analysis of strongly nonlinear response regimes, the computational expense associated with their application is often prohibitive for random analysis. Consequently, a nonlinear modal transformation from the analysis in physical degrees of freedom (DOF) to one in modal coordinates is sought to reduce the system size. Over the years, time-domain FE-based nonlinear reduced-order simulation methods have been extensively developed for application to a diverse spectrum of dynamic response problems [1]. It has been shown that accurate predictions may be made provided that an adequate modal basis is used in the nonlinear modal transformation [2–5]. A recently developed procedure for selecting such a basis [2,5] was found to compare well with full-order simulations over a broad intensity range of spatially invariant loading conditions when the worst-case loading scenario is used in the identification process. Cases with time-varying loading distributions, however, have received little attention. In such cases, the difficulty in developing a robust nonlinear reduced-order basis stems from the fact that the desired modal basis is changing with time and, consequently, the worst-case loading scenario is not intuitive.

The present work expands application of a the modal basis procedure [2,5] to the analysis of problems with time-varying spatial loading distributions. The procedure is based on system identification via proper orthogonal decomposition (POD) [6,7]. The proper orthogonal modes (POMs), however, change with loading distribution and intensity, and so they do not constitute an efficient basis. Therefore, an additional step involving modal expansion seeks to identify normal modes (NMs) resembling POMs. In the past, a basis formed using NMs was found to be applicable over a broad range of response regimes having a fixed loading distribution [2,5].

In the present study, a basis that is also applicable over a perturbed set of spatially time-varying loading conditions is sought. By repeating the basis selection procedure, new NM bases may be found for perturbations of the spatially time-varying loading condition. Finally, because all the NMs are orthogonal, these bases may be combined to form a single NM basis applicable over the range of loading conditions analyzed. In doing so, a significant computational savings may be achieved.

To demonstrate that the proposed approach is applicable to time-varying spatial loading distributions, the focus of the present work is on a structure simultaneously subjected to an oscillating pressure gradient and high-intensity acoustic loading. This condition was motivated by oscillating shocks acting in combined thermal-acoustic loading environments, as encountered on hypersonic-flight vehicle structures [8]. Figure 1 depicts such a loading case, in which an oscillating shock formed ahead of a compression ramp [9,10] combines with an acoustic disturbance generated by a scramjet (supersonic combustion ramjet) propulsion system [8]. In such a scenario, the acoustic disturbance will forward-propagate only in the subsonic region aft of the shock. The effects of fluid and thermal loadings, although significant in the motivational problem, are not included in this study. The loading conditions considered are presented in Fig. 2. The oscillation boundary between the low static pressure P_o and the high static pressure P_1 moves with frequency f. The structure is modeled as a composite plate strip, and the strength of the pressure gradient and oscillation frequency were guided by available empirical data [9,10]. The reference condition is indicated as load case 1 in Table 1, and perturbations of selected parameters (including location, frequency, and span of the oscillating pressure gradient) are indicated as load cases 2–7.

II. Formulation

The system identification employed by the authors [5] is next reviewed and a modal basis selection criterion employing a modal expansion approach [2] is summarized. The previously developed modal system reduction by an indirect nonlinear stiffness evaluation procedure [4,11] is also briefly discussed.

A. System Identification: Proper Orthogonal Decomposition

When physical DOF are chosen to characterize the response, a snapshot matrix $[X]$ can be formed as an accumulation of n instantaneous displacement, velocity, or acceleration response fields [6,7]. In the current analysis, displacement fields obtained from a full-order nonlinear FE analysis are used, resulting in a snapshot matrix of size $n \times N$, where N is the number of DOF. The sample rate and spatial resolution of the snapshot matrix must be sufficient to resolve the system's temporal and spatial characteristics of interest. The correlation matrix $[R]$, of size $N \times N$, is formed as

$$[R] = \frac{1}{n}[X]^T[X] \tag{1}$$

An eigenanalysis of the correlation matrix is next performed: that is,

$$([R] - [\lambda][I])\{p\} = \{0\} \tag{2}$$

to obtain a POM matrix $[P] = [\{p_1\} \quad \{p_2\} \quad \dots \quad \{p_N\}]$ and the diagonal proper orthogonal value (POV) matrix $[\lambda]$, both of size $N \times N$. Each POV is a measure of the corresponding POM activity; that is, the higher the POV, the greater the contribution of a corresponding POM to the dynamic response.

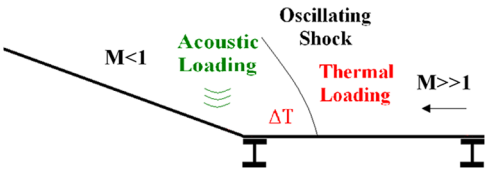

Fig. 1 Oscillating shock due to hypersonic flow over compression ramp.

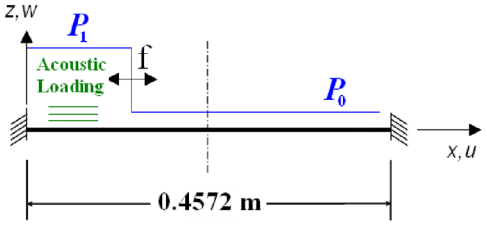

Fig. 2 Composite plate strip under simplified time-varying spatial loading distribution.

The POD procedure employed is performed independently for each DOF type of interest by partitioning the snapshot matrix. In the subsequent POD analyses, three out of six available DOF types for shell FEs are considered: namely, transverse displacement w and two in-plane displacements u and v. The two out-of-plane rotations ψ_x and ψ_y were previously found [2] to ultimately yield the same set of NMs as the transverse displacement DOF, and so they are not considered in the present analysis. The sixth DOF type, the rotation about the normal to the plate surface ψ_z, commonly referred to as the drilling DOF, also is not considered because it is not common to all shell element formulations. By adopting this approach, the size of each individual DOF snapshot matrix $[X]$ is reduced to $n \times m$, where m is the number of nodes, and the size of each individual correlation matrix $[R]$, POM matrix $[P]$, and POV matrix $[\lambda]$ is reduced to $m \times m$.

B. Modal Basis Selection

The contribution of each POM to the overall dynamic response is given by

$$\chi_i = \lambda_i \Big/ \sum_{j=1}^{m} \lambda_j \qquad i = 1, \dots, m \tag{3}$$

where χ_i is the ith POM participation factor. The sum of all POM participation factors is unity. When the most contributing M POMs are selected, their cumulative participation υ can be expressed as

$$\upsilon = \sum_{i=1}^{M} \chi_i \qquad 0 < \upsilon \leq 1 \tag{4}$$

Retention of only the selected M POMs reduces the size of $[P]$ to $m \times M$.

As previously indicated, the direct use of POMs for the basis is not preferred for a forced response problem, as they are load-specific. Instead, a set of NMs that either directly resemble or can be superposed to resemble the POMs is sought. The authors recently presented two criteria for identifying such a set using the modal assurance criterion (MAC) [12] and a modal expansion approach [2]. Because of the loading considered, the POMs identified in this work often bore little direct resemblance to NMs. Consequently, the MAC approach was not generally effective and is therefore not considered in this paper.

A single POM may be decomposed into a linear superposition of NMs using the expansion [13]

$$\{p_i\} = \sum_{j=1}^{L} c_{ij}\{\phi_j\} \tag{5}$$

where c_{ij} are the expansion coefficients. Because the NMs $\{\phi\}$ are orthogonal, that is,

$$\{\phi_k\}^T\{\phi_l\} = \{0\} \qquad k \neq l \tag{6}$$

premultiplying Eq. (5) by $\{\phi_k\}^T$ yields

$$s_{ik} = c_{ik}\{\phi_k\}^T\{\phi_k\} = \{\phi_k\}^T\{p_i\} \tag{7}$$

The coefficient matrix $[S]$ may be formed by evaluating Eq. (7) over all selected POMs ($i = 1, \dots, M$) and over all NMs ($k = 1, \dots, N$) and may be written in compact form as

Table 1 Time-varying spatial loading distributions

Load case	Oscillation span, mm	Oscillation center position x, mm	Oscillation frequency, Hz	Max. oscillation speed, m/s
1	12.7	114.30	714.0	28.49
2	12.7	57.150	714.0	28.49
3	12.7	171.45	714.0	28.49
4	63.5	114.30	142.8	28.49
5	127.	114.30	7.140	2.849
6	127.	114.30	71.40	28.49
7	127.	114.30	714.0	284.9

$$[S] = [\Phi]^T[P] \tag{8}$$

One $[S]$ matrix is formed for every DOF type, and the size of each $[S]$ matrix is $N \times M$.

Each column of $[S]$ corresponds to a specific POM. Because the POMs $[P]$ used to compute the $[S]$ matrix are not normalized, it is convenient to normalize each column of this matrix to unity so that a single threshold value can be used to identify the most significant NMs. As such, the modal expansion approach is guaranteed to identify at least one NM. In this work, those modes above a threshold value of 0.5 were included in the basis.

C. Nonlinear Reduced-Order Analysis

Once a set of basis functions consisting of NMs is selected using modal expansion, the nonlinear modal reduction of the system can proceed. A reduced-order method gains its computational advantage by reducing the size of the system in physical DOF (full-order) to a much smaller system expressed in generalized coordinates (reduced-order). For the problem of interest, the equation of motion in physical DOF is expressed as

$$[M]\{\ddot{x}(t)\} + [C]\{\dot{x}(t)\} + \{f_{NL}(x(t))\} = \{f(t)\} \tag{9}$$

where $[M]$ and $[C]$ are the structural mass and damping matrices, and $\{x\}$, $\{f_{NL}\}$, and $\{f\}$ are the physical displacement, nonlinear restoring force, and excitation force vectors, respectively. By applying the modal transformation

$$\{x(t)\} = [\Phi]\{q(t)\} \tag{10}$$

the equation of motion is expressed in reduced-order form as

$$[\tilde{M}]\{\ddot{q}(t)\} + [\tilde{C}]\{\dot{q}(t)\} + \{\tilde{f}_{NL}(q_1(t), q_1(t), \ldots, q_L(t))\} = \{\tilde{f}(t)\} \tag{11}$$

where $\{q\}$ is a generalized coordinate vector and $[\Phi]$ is a matrix containing L selected NMs of the basis. The modal nonlinear restoring force in Eq. (11) is obtained by

$$\{\tilde{f}_{NL}\} = [\Phi]^T\{f_{NL}\} \tag{12}$$

Because mass-normalized NMs are used as the basis functions, the modal mass and damping matrices can be expressed as

$$[\tilde{M}] = [\Phi]^T[M][\Phi] = \lceil I \rfloor \qquad [\tilde{C}] = [\Phi]^T[C][\Phi] = \lceil 2\zeta_r\omega_r \rfloor \tag{13}$$

where ω_r and ζ_r are the undamped natural frequencies and the viscous damping factors, respectively. The modal excitation force vector is given by $\{\tilde{f}(t)\} = [\Phi]^T\{f(t)\}$.

The system reduction used in this study is based on the indirect approach employing a nonlinear stiffness evaluation procedure [4,11]. The procedure expresses the rth component of the nonlinear modal restoring force vector as

$$\tilde{f}^r_{NL}(q_1, \ldots, q_L) = \sum_{j=1}^{L} d^r_j q_j + \sum_{j=1}^{L}\sum_{k=j}^{L} a^r_{jk} q_j q_k + \sum_{j=1}^{L}\sum_{k=j}^{L}\sum_{l=k}^{L} b^r_{jkl} q_j q_k q_l \qquad r = 1, \ldots, L \tag{14}$$

where d, a, and b are the linear, quadratic, and cubic modal stiffness coefficients. Different combinations of scaled NMs form a set of prescribed displacement fields. The normal mode vectors are scaled by the generalized coordinates $\{q\}$ to obtain physically meaningful magnitudes. Using a nonlinear static FE analysis, the nonlinear restoring forces corresponding to each prescribed displacement field are computed in physical DOF and transformed to the generalized coordinates per Eq. (12). As the vector $\{f_{NL}\}$ and the generalized coordinates $\{q\}$ are known, Eq. (14) constitutes a system of algebraic equations from which the linear, quadratic, and cubic modal stiffness coefficients may be determined. The number of unknown coefficients, and hence the number of nonlinear static solutions required for a transformation using L modes, is

$$3\binom{L}{1} + 3\binom{L}{2} + \binom{L}{3} \qquad L \geq 3 \tag{15}$$

where

$$\binom{L}{k} = \frac{L!}{k!(L-k)!} \tag{16}$$

Note that the three terms in Eq. (15) reflect the number of linear, quadratic, and cubic modal stiffness coefficients, respectively. The number of nonlinear static solutions can be viewed as a measure of the fixed cost of the reduced-order analysis, as the modal reduction must be performed regardless of the simulated response time to be eventually computed. Once the coefficients have been determined, Eq. (11) is integrated using a fourth-order Runge–Kutta scheme and the physical displacements recovered through Eq. (10). The reduced-order analysis was implemented in the code RANSTEP [4], which can use either the ABAQUS [14] or MSC.Nastran [15] FE codes for NM analysis, nonlinear static solutions, and stress/strain postprocessing.

III. Results

The FE model developed for the ensuing numerical analyses is next presented. The process for generating the time-varying spatial loading distribution follows, with particular attention paid to the high-frequency components generated in the region of pressure oscillation. A thorough treatment of a reference load case is then considered to lend insight into the selection of a modal basis using the preceding approach and to demonstrate the accuracy of a reduced-order nonlinear simulation vis-à-vis a full-order simulation. Loading parameters are next perturbed to investigate the influence of oscillation position, frequency, and span on the response and modal basis selection. Finally, the computational effort associated with a robust expanded modal basis is addressed.

A. Finite Element Model and Analyses

A graphite-epoxy composite plate strip clamped at both ends served as the numerical test article. The structure under investigation,

shown in Fig. 2, measured $457.2 \times 25.4 \times 2.0$ mm (length by width by height). Sixteen 0.125 mm layers are stacked in the lamination sequence $(45/0/-45/90/45/0/-45/90)_s$. Because the laminate was symmetric, there was no material bending/extensional coupling. Material properties used for the graphite-epoxy lamina were Young's modulus $E_1 = 181.1$ GPa and $E_2 = 10.3$ GPa, Poisson's ratio $\upsilon_{12} = 0.28$, shear modulus $G_{12} = G_{13} = G_{23} = 7.17$ GPa, and mass density $\rho = 1550$ kg/m^3. The mass proportional damping of $C = 11.223$ 1/s was applied, and the value corresponded to 1.3% critical damping of the first symmetric transverse mode at $f_1 = 68.7$ Hz.

A single FE model of the plate strip was constructed for both the full-order and reduced-order analyses. It consisted of 1216 ABAQUS S4R shell elements defined by 1525 nodes for a total of 9150 DOF. The S4R element has four nodes, each with three translational and three rotational DOF. All elements used had a width of 6.35 mm, so that four elements spanned the width of the strip. The length of the elements was either 3.125 or 0.635 mm. The smaller element length was used over the greatest region of oscillating pressure loading (i.e., from 50.8 to 177.8 mm).

The full-order nonlinear response of the plate strip was analyzed in physical DOF using the ABAQUS/Explicit solution. Because of the small element size used in the region of pressure oscillation, the automatic element-by-element time-step selection scheme used in ABAQUS yielded an extremely small integration time step of 55.54×10^{-9} s. Hence, the full-order simulations were computationally very intensive, making only short time simulations feasible. The reduced-order analyses were performed with a much larger integration time-step increment of 1.25×10^{-6} s.

B. Load Generation

The beam was subjected to a static pressure loading of $P_o = 1$ kPa ahead (to the right) of the lateral pressure oscillation boundary and a static pressure loading of $P_1 = 10$ kPa behind (to the left of) the lateral pressure oscillation boundary (see Fig. 2). This pressure rise is on the order of that cited by Elfstrom [10] for a hypersonic Mach number of 9.22 flow incident upon a 15 deg compression wedge. The pressures P_o and P_1 were applied uniformly across the width and the affected length of the strip. The pressure oscillation boundary between P_o and P_1 moved in a sinusoidal fashion, at frequencies indicated in Table 1. In the region of travel, the instantaneous resultant force was calculated and applied proportionally across the nearest element nodes. This representation of the oscillating load was mathematically convenient to implement and was not intended to precisely model an oscillating shock. In addition, a uniformly distributed random acoustic loading of 160 dB overall sound pressure level (reference pressure 20 μPa) over the frequency range 0–1024 Hz was applied behind the pressure oscillation boundary. The acoustic pressure tracked left and right with the boundary movement such that no acoustic loading was applied ahead of the boundary.

The pressure–time history in the midspan region of oscillation is shown in Fig. 3 for an oscillation span of 63.5 mm and frequency of 142.8 Hz (load case 4). At this location, the oscillation boundary reaches its maximum oscillation speed of 28.49 m/s. The pressure–time history is shown both with and without the acoustic loading to demonstrate the modulation induced by the acoustic loading on the 10 kPa static pressure behind the oscillation boundary. The transition between high and low pressure occurs over a short period of time, such that the resulting pressure–time history resembles a square wave. The effect of the pressure oscillation is dramatically shown in its power spectral density (PSD) in Fig. 4. Because the waveform is essentially square, spectral peaks are generated at the oscillation frequency and its odd harmonics. The peaks extend to very high frequencies (greater than 40 kHz). The most noticeable effect is the generation of high-frequency broadband noise above the acoustic loading cutoff of 1024 Hz, as shown by the trace referenced as 160 dB + 63.5 mm/142.8 Hz Osc (oscillation). This distortion occurs as a result of chopping the acoustic loading. Because the midspan region of oscillation is exposed to 160 dB for only half of each oscillation cycle, the time-averaged exposure is reduced by 3 dB

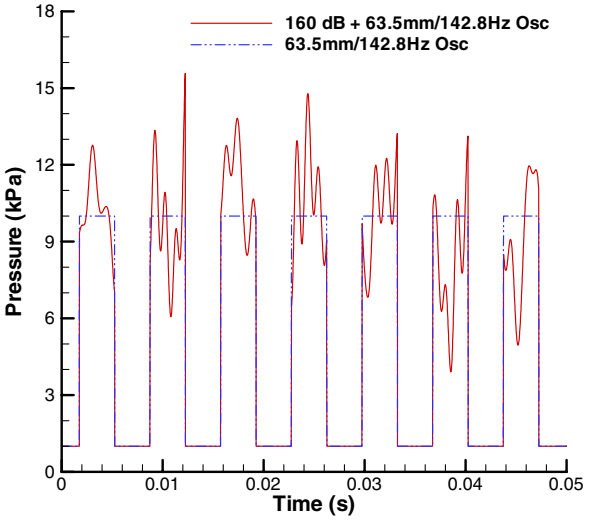

Fig. 3 Unsteady pressure–time history for load case 4 both with and without the 160 dB acoustic loading.

relative to the full level. This is most clearly seen through comparison of the in-band (0–1024 Hz) acoustic spectrum with and without the oscillation, shown by the trace referenced as 160 dB+ 63.5 mm/142.8 Hz Osc and by the trace referenced as 160 dB (0–1024 Hz), respectively. Although the overall acoustic component is reduced, the combined overall level (broadband acoustic and spectral peaks) is increased by roughly 7 to 167 dB, not including the sizeable zero-frequency component. This behavior was found to exist for all load cases, each of which had comparable amplification but differing peak behaviors. Because the integrated amplification is the same irrespective of the oscillation frequency, lower oscillation frequencies have lower amplitudes, because more harmonics are integrated over the given bandwidth than with a higher-frequency oscillation. For example, the amplitude of a 7.14 Hz oscillation is lower than that of the 71.4 Hz oscillation.

The net effect of the distorted fluctuating pressure loading on the structural response is twofold. First, spectral peaks, though narrow, have the potential to cause large structural dynamic response if located in the vicinity of a structural resonance. Second, the high-frequency content of the loading will excite a greater number of low-frequency bending NMs, compared with the undistorted acoustic spectrum, and has the potential to directly excite higher-frequency in-plane NMs. The anticipated result is that a larger modal basis will be required for the reduced-order analysis, compared with a basis required for acoustic loading only.

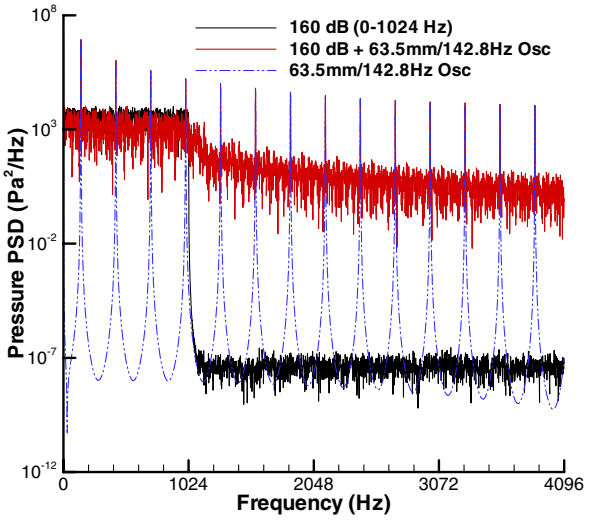

Fig. 4 Pressure PSD for load case 4 with and without the 160 dB acoustic loading.

C. Analysis of Reference Condition: Load Case 1

For the POD analysis of the reference condition and perturbed load cases (see Table 1), a single 1.0 s full-order nonlinear response simulation was run with an output interval of 50 μs. In each case, the first 0.5 s of response was removed to minimize the effect of startup transients. Thus, the POD analyses were performed using $n = 10,000$ full-field displacement snapshots. Displacement response PSDs (Figs. 5–9) were computed using simulations extended to 2.1384 s, giving 1.6384 s of evolved response for computation of the PSD to provide an enhanced frequency resolution.

Also common to all load cases was the selection of a cumulative POV contribution υ of 99.9% for the u and v displacement components and of 99.999% for the w displacement component. The higher value for the w displacement component was selected to help identify additional low-frequency bending NMs that lie above the direct acoustic loading bandwidth of 1024 Hz. The contribution of such modes has been previously found to be important [2,5].

The POD analysis for the reference condition identified 21 POMs falling within the cumulative POV contribution values selected. Of these, 10 were associated with the u displacement component, 3 with the v displacement component, and 8 with the w displacement component. A listing of POMs and their individual and cumulative contributions is provided in Table 2. It is seen that the w displacement component converges faster than the u displacement component for a

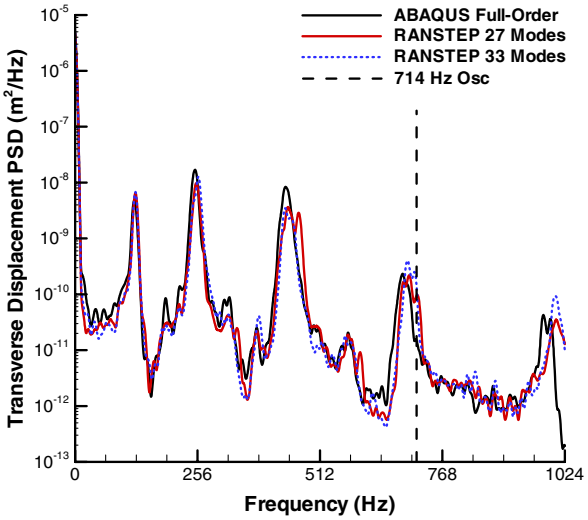

Fig. 5 Transverse displacement PSD at quarter-span location for load case 1.

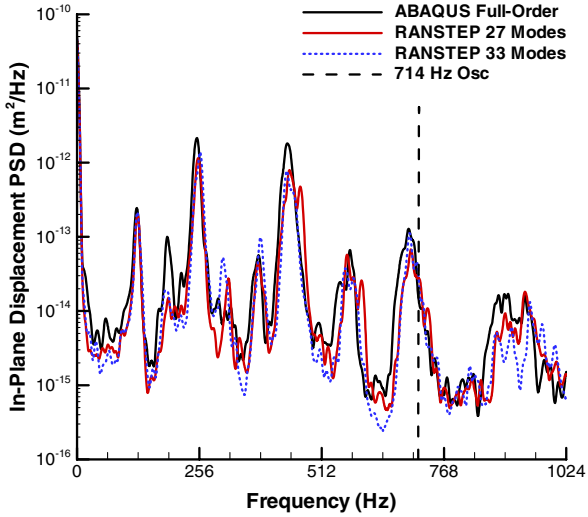

Fig. 6 In-plane displacement PSD at the quarter-span location for load case 1.

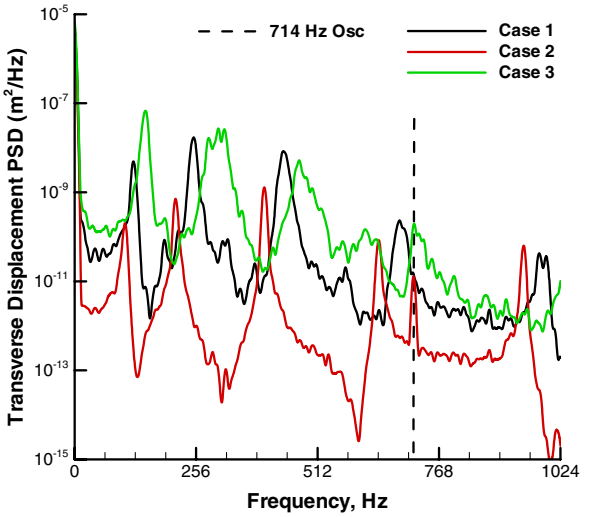

Fig. 7 Effect of oscillation center position on the quarter-span transverse displacement PSD.

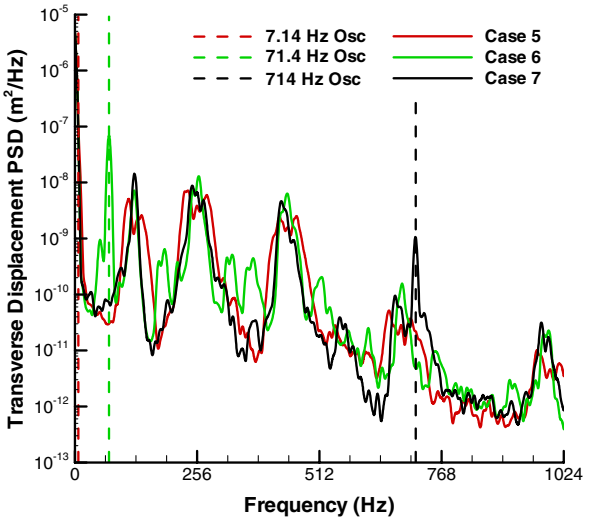

Fig. 8 Effect of oscillation frequency on the quarter-span transverse displacement PSD.

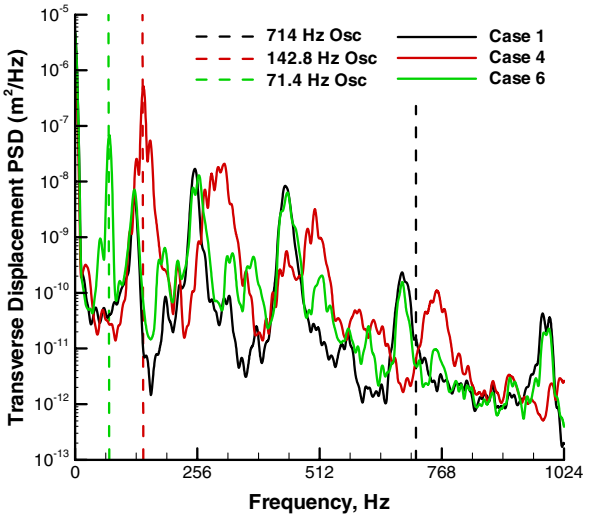

Fig. 9 Effect of oscillation span on the quarter-span transverse displacement PSD.

Table 2 POVs and NMs identified for the reference condition (load case 1)

POM displacement component	POM Number	POV contribution, %	Cumulative POV contribution, %	NM no. identified via modal expansion
u	1	79.7987	79.799	29, 45, 65
u	2	8.8265	88.625	29, 45, 87
u	3	6.2354	94.861	6, 237, 240
u	4	1.9823	96.842	65
u	5	1.7508	98.594	87, 105
u	6	0.6696	99.263	87, 105, 119, 176, 198
u	7	0.3600	99.623	119, 135, 198
u	8	0.1729	99.796	148
u	9	0.0850	99.881	105, 119, 135, 176
u	10	0.0559	99.937	11, 41, 237, 245
v	1	98.8873	98.887	6, 11
v	2	0.09065	99.794	11, 19
v	3	0.01481	99.942	19, 26
w	1	91.0671	91.067	1, 2, 3
w	2	5.4295	96.497	2, 3, 4
w	3	2.7486	99.245	2
w	4	0.5409	99.786	4, 7
w	5	0.1344	99.920	7
w	6	0.0669	99.987	5, 9
w	7	0.0111	99.998	9
w	8	0.0009	99.999	8, 10

cumulative POV contribution of 99.9% (5 POMs for the w displacement and 10 POMs for the u displacement). This is consistent with earlier work on beam and plate structures subject to uniformly distributed loadings [2,5].

A list of selected NMs and their types (spanwise symmetric or antisymmetric) is provided in Table 3. Individual columns in Table 3 indicate the basis identified for a specific loading case (numbers 1 through 7) and are subsequently referred to as the *individual* bases. The number of unique NMs spanning all load cases in Table 3 is subsequently referred to as the *cumulative* basis. The concept of a cumulative basis is further discussed in Sec. III.E. Only NMs in the frequency bandwidth to 90 kHz were considered in this study.

The PSDs of the quarter-span transverse displacement response computed using full-order and reduced-order nonlinear simulations using 27 modes (individual basis) and 33 modes (cumulative basis) are presented in Fig. 5. The frequency resolution for this and subsequent PSD plots was 0.61 Hz. The quarter-span location was chosen to monitor the solution quality because it lies in the middle of the most severe loading. Both reduced-order simulations compare favorably with the physical DOF simulation, as they capture both the zero-frequency behavior associated with the static pressure loading and the higher-frequency response. Figure 6 shows the quarter-span in-plane displacement PSD, for which the amplitude is about 4 orders of magnitude lower than that of the transverse response. Again, both reduced-order analyses compare favorably with the full-order analysis across the frequency range. Similar to the transverse displacement results, no significant differences between the two reduced-order analyses are noted. In both the transverse and in-plane responses, the forced response at the excitation oscillation frequency is not prominent because of the low admittance of the system at this frequency.

From the data presented in Figs. 5 and 6, several important conclusions can be made. The most significant is that the reduced-order analysis embodied in this work is capable of modeling time-varying spatial loading distributions provided that an adequate basis is used. Next, the combination of POD and modal expansion has been shown to be effective for identifying such a basis. Finally, because the loading contains high-frequency components and is spatially concentrated, the modal basis is larger than that required for a uniformly distributed loading with lower-frequency content [3].

D. Perturbations of Oscillation Position, Frequency, and Span

To determine the requirements for an expanded basis applicable over perturbed loading conditions, and at the same time gain further insight into the nonlinear structural dynamic response associated with this problem, the effects of varying the oscillation center position, frequency, and span were investigated.

1. *Effect of Oscillation Center Position*

The effect of the oscillation center position was investigated by perturbing the 114.3 mm center position (load case 1) nearer to the left clamped end at spanwise location 57.15 mm (load case 2) and nearer to the center at spanwise location 171.45 mm (load case 3), while maintaining an oscillation span of 12.7 mm and oscillation frequency of 714 Hz.

The quarter-span transverse displacement PSDs obtained from the full-order analyses are shown in Fig. 7. For load case 2, the structure has the least amount of exposure to the high-amplitude static pressure P_1; consequently, the stiffening effect due to application of the static pressure is less than it is for load cases 1 and 3. Therefore, its resonances are only slightly shifted to the higher frequencies, relative to the unstressed natural frequencies indicated in Table 3. The area of applied static pressure P_1 increases for load case 1 and is greatest for load case 3, and so the frequency shift is progressively greater. Even though the plate strip is stiffest for case 3, followed by case 1, followed by case 2, the amplitude of the response has the opposite trend. It is greatest for case 3, followed by case 1, followed by case 2. This is because the acoustic loading area also increases as the center of oscillation moves from left to right. The 714 Hz oscillation frequency is clearly noticeable in load case 2 and barely noticeable in load case 3.

The POD/modal expansion analysis identified 24 NMs associated with 18 POMs for load case 2 and 28 NMs associated with 21 POMs for load case 3. The breakdown of POMs by component type for each load case is shown in Table 4, and the particular NMs identified for each case are indicated in Table 3. A general trend seen is that a lower response amplitude and a lesser stiffening effect result in a fewer POMs (and, consequently, fewer NMs) identified by the POD/modal expansion procedure. For linearly responding systems, the POM and NM shapes are usually very similar [7]. As the level of nonlinearity increases, differences between the shape of the POMs and NMs tend to increase and, consequently, more NMs are required to represent a strongly nonlinear POM.

It should be emphasized that the POMs differ between each load case: that is, the u component POM number 1 for load case 1 is different from the u component POM number 1 for load case 2. The NMs, however, are the same for each load case, as they are determined from the stress-free linear eigenanalysis. The fact that many of the same NMs are represented for differing load cases is why they are desirable for forming the cumulative basis.

Table 3 Selected (unstressed) NMs for each load case; NM selections common to all cases are indicated in bold

NM no./type [a]	Dominant displacement	Freq., Hz	Load case number						
			1	2	3	4	5	6	7
1 S	*w*	68.696	+	+	+	+	+	+	+
2 A	*w*	189.29	+	+	+	+	+	+	+
3 S	*w*	371.07	+	+	+	+	+	+	+
4 A	*w*	613.51	+	+	+	+	+	+	+
5 S	*w*	730.85	+	—	+	+	+	+	+
6 S	*v*	797.03	+	+	+	+	+	+	+
7 S	*w*	916.83	+	+	+	+	+	+	+
8 A	*w*	1281.2	+	+	+	+	+	+	+
9 A	*w*	1465.1	+	—	+	+	+	+	+
10 S	*w*	1706.7	+	+	+	+	+	+	+
11 A	*v*	2146.6	+	+	+	+	+	+	+
12 A	*w*	2190.1	—	—	+	—	—	—	+
14 S	*w*	2740.1	—	—	+	—	—	—	—
19 S	*v*	4087.0	+	+	+	+	+	+	+
21 A	*w*	4744.3	—	—	+	—	—	—	—
26 A	*v*	6527.7	+	+	+	+	+	+	+
29 A	*u*	7342.5	+	+	+	+	+	+	+
34 S	*v*	9387.3	—	+	—	—	—	—	—
41 A	*v*	12,591	+	+	—	—	—	—	—
45 A	*u*	14,682	+	+	+	+	+	+	+
65 S	*u*	22,015	+	+	+	+	+	+	+
87 A	*u*	29,337	+	+	+	+	+	+	+
105 S	*u*	36,644	+	+	+	+	+	+	+
119 A	*u*	43,930	+	+	+	+	+	+	+
135 S	*u*	51,186	+	+	+	+	+	+	+
148 A	*u*	58,403	+	+	+	+	+	+	+
176 S	*u*	65,566	+	+	+	+	+	+	+
198 A	*u*	72,656	+	+	+	+	+	+	+
217 S	*u*	79,644	—	+	—	—	—	—	+
234 A	*u*	86,491	—	—	—	—	—	—	+
237 S	*u*	86,907	+	—	+	+	+	—	+
240 A	*u*	88,131	+	—	+	+	+	+	+
245 S	*u*	89,881	+	—	—	—	—	—	—
		Total	27	24	28	25	25	24	28

[a]S is spanwise symmetric, and A is spanwise antisymmetric.

2. Effect of Oscillation Frequency

The oscillation frequency was varied by 2 orders of magnitude. Load cases 5 (7.14 Hz), 6 (71.4 Hz), and 7 (714 Hz) were compared to maintain the same oscillation center position and span. The quarter-span transverse displacement PSDs obtained from the full-order analyses are shown in Fig. 8. The transverse displacement responses for load cases 6 and 7 are significantly driven by the 71.4 and 714 Hz excitation oscillation frequencies, respectively. The 7.14 Hz driving frequency for load case 5 is not discernible near the dominant static response. Additional peaks in the response at the odd harmonics of the 7.14 and 71.4 Hz oscillation frequencies are not discernible.

The POD/modal expansion analysis identified 25 NMs associated with 20 POMs for load case 5, 24 NMs associated with 19 POMs for load case 6, and 28 NMs associated with 23 POMs for load case 7. The number of POMs of each type does not significantly differ, as shown in Table 4. Again, there is significant commonality between the corresponding sets of NMs seen in Table 3.

3. Effect of Oscillation Span

The effect of oscillation span was explored by perturbing load case 1 such that the span increased by a factor of 5 to 63.5 mm (load case 4) and by a factor of 10 to 127 mm (load case 6), while maintaining the oscillation center position at the quarter-span and maximum oscillation speed of 28.49 m/s. Because the oscillation speed was maintained, the oscillation frequency was reduced from 714 Hz for load case 1 to 142.8 Hz for load case 4 and to 71.4 Hz for load case 6. Therefore, this perturbation was not independent of a change in frequency.

The quarter-span transverse displacement PSDs obtained from the full-order analyses are shown in Fig. 9. Here, both the 71.4 and 142.8 Hz oscillation frequencies significantly drive the responses of load cases 6 and 4, respectively. Odd harmonics of the 71.4 and 142.8 Hz oscillation frequencies are again not discernible. The POD/modal expansion analysis identified 25 NMs associated with 21 POMs for load case 4 and 24 NMs associated with 19 POMs for load

Table 4 Summary of POMs and NMs for each loading case

Case	Number of *u* component POMs	Number of *v* component POMs	Number of *w* component POMs	Total number of	
				POMs	NMs
1	10	3	8	21	27
2	7	5	6	18	24
3	8	4	9	21	28
4	8	4	9	21	25
5	9	3	8	20	25
6	8	3	8	19	24
7	10	3	10	23	28

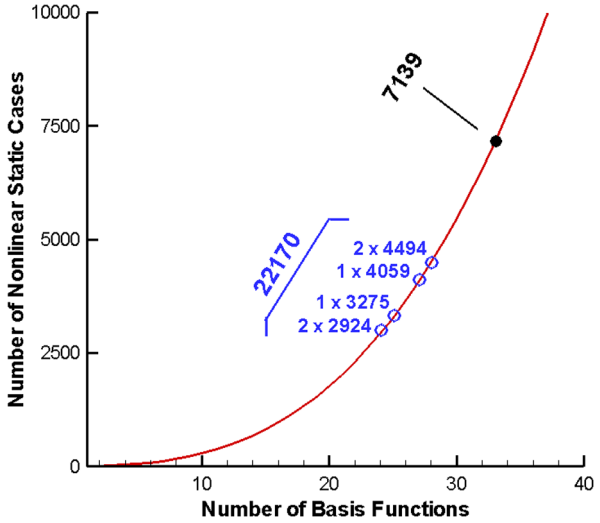

Fig. 10 Computation cost associated with individual and cumulative modal bases.

case 6. The number of POMs of each type does not significantly differ between load cases 4 and 6, as seen in Table 4. Again, there is significant commonality between the corresponding NMs seen in Table 3.

E. Computational Effort for Individual and Cumulative Modal Bases

If the seven loading conditions were considered individually, a separate reduced-order system would need to be formed for each using the modal bases presented in Table 3. Because load cases 4 and 5 resulted in the same NM basis selection (despite the fact that a different number of POMs were identified for these two load cases), only a single common reduced-order system needs to be formed for them. The computational effort associated with obtaining the reduced-order system for the resulting six different bases can be computed per Eq. (15). The number of static nonlinear cases to be solved for each is presented in Fig. 10 with the open circles. The total effort requires the solution of 22,170 static nonlinear cases.

In previous work, the authors demonstrated that expanding the modal basis does not adversely affect the quality of the reduced-order solution [5]. The same can be concluded from Figs. 5 and 6, in which the cumulative 33-mode basis was shown to give results comparable with the 27-mode individual basis. Because of this, only a single reduced-order system needs to be formed, with a cumulative basis consisting of a superset of all modes identified in Table 3. As a result, a reduced-order system with 33 modal basis functions can be obtained and applied for the analysis of any or all of the cases under consideration. The cost associated with forming such a system requires the solution of 7139 nonlinear static cases, as indicated with a black data point in Fig. 10. Consequently, the computational effort of modal reduction using a single cumulative basis is reduced by the factor of 3.1 relative to that of six individual reductions. Note that the extent of perturbations from the baseline condition affects the number of common NMs between cases and hence the efficiency to be gained by forming a common basis. For the seven cases considered in this work, 21 out of 33 NMs listed in Table 3 are common.

There are obstacles to using the POMs to form a cumulative modal basis. First, each set of POMs is load-case-specific. Therefore, a common basis would consist of all 143 POMs identified in Table 4 and would require the solution of 508,079 nonlinear static cases. Second, a basis formed in this manner would be composed of vectors that are generally not orthogonal. This has been shown to lead to difficulties in integrating the reduced-order system [3].

IV. Conclusions

A nonlinear reduced-order modal simulation has been demonstrated to accurately predict the response of structures with time-varying spatial loading distributions provided that an appropriate modal basis is selected. Selection of such a basis requires knowledge of the system dynamics that can be gained by a system identification procedure. The proper orthogonal decomposition used for this purpose leads to a set of proper orthogonal modes, and although these may be used directly to form a reduced-order system, such a system is load-specific. A load-independent basis, however, is more desirable, as it permits analysis of a broader range of loading conditions using the same reduced-order system.

A load-independent basis can be formed using normal modes that are identified via modal expansion of the proper orthogonal modes. By perturbing the baseline loading condition, the POD analysis and modal expansion can be repeated to incrementally expand the modal basis. The resulting cumulative basis was demonstrated to be more computationally efficient than independent analyses of all perturbed conditions.

References

[1] Hollkamp, J. J., Gordon, R. W., and Spottswood, S. M., "Nonlinear Modal Models for Sonic Fatigue Response Prediction: A Comparison of Methods," *Journal of Sound and Vibration*, Vol. 284, No. 3–5, 2005, pp. 1145–1163. doi:10.1016/j.jsv.2004.08.036

[2] Przekop, A., and Rizzi, S. A., "Efficient Modal Basis Selection Criteria for Reduced-Order Nonlinear Simulation," EURODYN 2008, 7th European Conference on Structural Dynamics, Southampton, England, U.K., European Association for Structural Dynamics, Paper E69, 2008.

[3] Rizzi, S. A., and Przekop, A., "The Effect of Basis Selection on Static and Random Response Prediction Using Nonlinear Modal Simulation," NASA TP-2005-213943, Dec. 2005.

[4] Rizzi, S. A., and Przekop, A., "Estimation of Sonic Fatigue by Reduced-Order Finite Element Based Analyses," International Conference on Structural Dynamics: Recent Advances, Southampton, England, U.K., Inst. of Sound and Vibration Research Paper 128, 2006.

[5] Rizzi, S. A., and Przekop, A., "System Identification-Guided Basis Selection for Reduced-Order Nonlinear Response Analysis," *Journal of Sound and Vibration*, Vol. 315, No. 3, 2008, pp. 467–485. doi:10.1016/j.jsv.2007.12.031

[6] Feeny, B. F., and Kappagantu, R., "On The Physical Interpretation of Proper Orthogonal Modes in Vibrations," *Journal of Sound and Vibration*, Vol. 211, No. 4, 1998, pp. 607–616. doi:10.1006/jsvi.1997.1386

[7] Feeny, B. F., "On Proper Orthogonal Co-Ordinates as Indicators of Modal Activity," *Journal of Sound and Vibration*, Vol. 255, No. 5, 2002, pp. 805-817. doi:10.1006/jsvi.2001.4120

[8] Blevins, R. D., Bofilios, D., Holehouse, I., Hwa, V. W., Tratt, M. D., Laganelli, A. L., Pozefsky, P., and Pierucci, M., "Thermo-Vibro-Acoustic Loads and Fatigue of Hypersonic Flight Vehicle Structure—Phase II Report," ROHR Industries, Inc., Rept. CA RHR 89-202, Chula Vista, CA, 1989.

[9] Dolling, D. S., and Murphy, M. T., "Unsteadiness of the Separation Shock Wave Structure in a Supersonic Compression Ramp Flowfield," *AIAA Journal*, Vol. 21, No. 12, 1983, pp. 1628–1634. doi:10.2514/3.60163

[10] Elfstrom, G. M., "Turbulent Hypersonic Flow at a Wedge-Compression Corner," *Journal of Fluid Mechanics*, Vol. 53, No. 1, 1972, pp. 113–127. doi:10.1017/S0022112072000060

[11] Muravyov, A. A., and Rizzi, S. A., "Determination of Nonlinear Stiffness with Application to Random Vibration of Geometrically Nonlinear Structures," *Computers and Structures*, Vol. 81, No. 15, 2003, pp. 1513–1523. doi:10.1016/S0045-7949(03)00145-7

[12] Allemang, R. J., and Brown, D. L., "A Correlation Coefficient for Modal Vector Analysis," *Proceedings of the International Modal Conference*, Union College, Schenectady, NY, 1982, pp. 110–116.

[13] Doyle, J. F., *Static and Dynamic Analysis of Structures with an Emphasis on Mechanics and Computer Matrix Methods*, Kluwer Academic, Dordrecht, The Netherlands, 1991.

[14] ABAQUS, Software Package, Ver. 6.6, Abaqus, Inc., Providence, RI, 2005.

[15] MSC.Nastran, Software Package, Ver. 2005, MSC Software Corp., Santa Ana, CA, 2004.